Journal of Zhejiang University-SCIENCE A (Applied Physics & Engineering)
ISSN 1673-565X (Print); ISSN 1862-1775 (Online)
www.jzus.zju.edu.cn; www.springerlink.com
E-mail: jzus@zju.edu.cn

Sensitivity analysis and optimization design of hypoid gears' contact pattern to misalignments*

Xiao-le WANG[1], Jian-wei LU[†‡1], Shi-qin YANG[2]

[1]*School of Automotive and Transportation Engineering, Hefei University of Technology, Hefei 230009, China*

[2]*Research Center of Passenger Car, Anhui Jianghuai Automobile Co. Ltd., Hefei 230091, China*

[†]E-mail: jwlu75@hfut.edu.cn

Received Jan. 20, 2019; Revision accepted May 3, 2019; Crosschecked May 20, 2019

Abstract: Accurate evaluation of the misalignment sensitivity of hypoid gears is a significant foundation for analysis of its dynamics and for the calculation of machining parameters. A tooth contact analysis (TCA) methodology considering four kinds of misalignments is presented to calculate the contact pattern and transmission error. A sensitivity model of contact pattern to misalignments is established to investigate the effects of different alignment errors on meshing performance. By parameterizing the contact pattern, the influences of offset error, angular error, and the axial error of pinion and gear on the direction, shape, and position features of contact pattern are studied. Coefficients of four evaluation indexes to different misalignments are defined respectively, and the minimum sum of the weighted coefficients is utilized to establish a multi-objective comprehensive sensitivity model. Three curvatures of the pitch cone of the pinion are taken as the control variables, and a global selection space is then built within the reasonable range of those curvatures. An improved multi-population genetic algorithm (MPGA) is used to find the optimal set of curvatures to achieve the minimum synthetic sensitivity. TCA results indicate that the offset error and angular error have the greatest influence on the contact pattern. By adopting this methodology appropriately, the sensitivity of the contact pattern to misalignments can be reduced. The contributions of this paper can be summarized as: (1) an accurate parameterized measurement model of the contact pattern; (2) a comprehensive sensitivity model of the contact pattern to misalignments; (3) an optimization framework consisting of a calculation model of the machining parameters, a TCA model considering misalignments, and a misalignment sensitivity evaluation model.

Key words: Hypoid gear; Misalignment; Tooth contact analysis (TCA); Sensitivity analysis; Multi-population genetic algorithm (MPGA); Multi-objective optimization

https://doi.org/10.1631/jzus.A1900021 **CLC number:** TH132.41

1 Introduction

Current research on the optimization of the meshing performance of hypoid gears mainly focuses on theories of optimal design of tooth surfaces, and advanced manufacture and tooth contact analysis (TCA) technology (Bracci et al., 2009; Ding et al., 2016; Guo et al., 2016; Wang et al., 2016; Zhuo et al., 2017). As a primary tool for analyzing the meshing qualities of hypoid gears, TCA usually refers to the unloaded contact analyses of the gear pair, including the contact pattern analysis and transmission error (TE) analysis (Litvin et al., 1987; Litvin and Fuentes, 2004). The tooth contact pattern can show the load distribution on the mating surfaces visually, while TE is a metric generally used to evaluate the kinematic stability of the gear drive (Litvin et al., 1991; Vogel et al., 2002). In fact, the contact pattern and TE are jointly

‡ Corresponding author

* Project supported by the National Natural Science Foundation of China (No. 51875150), the Aeronautical Science Foundation of China (No. 2018ZEP4006), the Program for New Century Excellent Talents in University (No. NCET-10-0358), and the Major Projects of Natural Science Research for Universities in Anhui Province, China

ORCID: Xiao-le WANG, https://orcid.org/0000-0002-3516-3366

determined by the design principle, machining accuracy, and installation errors (Fan and Wilcox, 2007).

Originally, Gleason Works, USA developed a local conjugate theory (LCT) to control the meshing quality by observing the contact pattern on tooth surfaces directly, and the contact pattern was usually controlled in the middle of the tooth surface to accommodate different load conditions (The Gleason Works, 1971; Stadtfeld, 1993). Later, Litvin and Fuentes (2004) presented a local synthesis method (LSM) that established a relationship between the local geometry and relative motion of the mating surfaces at the calculation point, in which the contact patterns were used to evaluate the meshing quality. In (Achtmann and Bär, 2003), a series of determined bearing ellipses were adopted to represent the contact pattern, the position, shape, and inclination of which have been worked out respectively. Based on these data, an influence function was designed that described the effects of the supplemental flank correction motions on tooth contact states. Artoni et al. (2008) proposed an approach to automatically optimize the loaded contact pattern of spiral bevel gears. By improving the results of TCA, an optimal design of hypoid gears can be achieved (Mermoz et al., 2013).

Misalignments of a gear drive are the deviations of the gears from their ideal positions relative to each other, which can affect the load distribution and consequently the stress distribution on the full tooth surface. Due to machining errors, installation errors, and fluctuating loads, a hypoid gear drive inevitably operates with misalignments. Baxter and Spear (1961) studied the sensitivity of the curved-teeth bevel gear pair and used a "4×2" matrix to express the effects of a number of second-order meshing parameters on the sensitivities of installation errors. Based on the TCA approach, Litvin et al. (1995) researched the effects of misalignments on the transmission error and other meshing properties of hypoid gears, and then proposed a new method for absorbing the influences of installation errors by predetermining a parabolic TE function. Simon (1996) performed a TCA calculation on a pair of mismatched hypoid gears. He then studied the effects of misalignments of the pinion on meshing properties, and concluded that mounting errors may cause edge contact, and considerably worsen the conjugate state of the meshing surfaces, and thus worsen the load distribution (Simon, 1998). Simon (2008) studied the influences of misalignments on the contact stress, bending stress, and loaded transmission error, and proposed an optimization method to reduce the sensitivity of alignment errors. Gabiccini et al. (2010) made an automatic program to optimize the loaded contact pattern of face-milled hypoid gears with the consideration of mounting errors varying within prescribed ranges. Hotait et al. (2011) studied the effects of misalignments on tooth root stresses of hypoid gears experimentally, then proposed a model to predict the root stresses of face-milled and face-hobbed hypoid gears under various bearing and mismatching conditions. Simon (2014) presented an optimization approach for defining the optimal cutter geometry and machine-tool settings for reducing the sensitivity of spiral bevel gears to mounting errors. He studied how to apply this approach to minimize the effects of misalignments on the elasto-hydrodynamic lubrication features of spiral bevel gears.

Misalignment sensitivity analysis requires accurate description of contact characteristic parameters and relative mounting positions. Parametric modeling of the contact pattern and detailed discrimination of the effects of different alignment errors are necessary but are rare at present. In addition, previous studies mainly focused on how to evaluate and reduce the effects of misalignments on meshing properties, while ignoring analysis of the sensitivity of the contact pattern to mounting errors. Moreover, after analyzing the influences of misalignments, most studies focused on how to improve the meshing quality, while neglecting the elimination of adverse contact states, such as edge and corner contact states. Actually, due to the change of the load and assembly state, the real contact pattern may move to the edge of the tooth surface, which may lead to the failure of the optimization (Deng and Wei, 2012; Wang et al., 2018). In this paper, a TCA methodology considering four kinds of misalignments is presented to obtain a contact pattern and a TE curve. An accurate measurement model of the contact pattern is established. After that, a sensitivity model of the contact pattern to misalignments is established for studying the effects of four kinds of mounting errors on meshing properties. Both the contact pattern and the TE curve discussed in this paper are calculated from the unloaded TCA, which is a common tool used to evaluate the geometric contact characteristics of hypoid gears. Therefore, the effects of gear material on the meshing performance

are not covered in this study. Similarly, for the loaded tooth contact analysis, such as the effects of changes of the contact pattern on friction, pressure, scars, and other contacting characteristics, which are not studied in this paper, reference should be made to the following (Xu and Kahraman, 2007; Kolivand and Kahraman, 2009; Fan, 2011; Mohammadpour et al., 2014; Elisaus et al., 2017; Vivet et al., 2018). With respect to the above review of the literature, the contribution of this paper can be summarized as: (1) an accurate parameterized measurement model of the contact pattern is established; (2) a comprehensive sensitivity model of contact pattern to misalignments is built; (3) an optimization framework consisting of the calculation model of the machining parameters, a TCA considering alignment errors, and a misalignment sensitivity evaluation model is constructed.

2 Parametric description of misalignments and contact pattern

Due to processing errors, installation errors, and different load states, the position, shape, and direction of contact patterns on tooth surfaces are uncertain, which complicates the evaluation and analysis of the influences of misalignments. Hence, parametric modeling of misalignment and contact patterns is necessary for evaluating the meshing properties.

2.1 Equivalent misalignments

According to ANSI/AGMA 2008-C01 Assembling Bevel Gears (ANSI-AGMA, 2008), four types of installation errors need to be controlled when hypoid gears are mounted on a machine: the pinion axial error H_P, the gear axial error H_G, the offset error V, and the angular error Σ between the pinion axis and the gear axis, as shown in Fig. 1. Similarly, Litvin et al. (1995) also used these four misalignments to describe the installation errors of a hypoid gear pair. We thus chose these four types of misalignments for study.

2.2 Parametrization of the contact pattern

Based on Hertzian contact theory, the instantaneous contact area on a tooth surface can be approximated as an elliptical shape. However, with the movement of the instantaneous contact area on the tooth surface, what will eventually form on the entire tooth surface will be a rectangular or curvilinear shape. Parametric characteristics of the contact pattern include the direction angle γ_{cp}, the area S_{cp}, and the coordinate $[x_{cp}, y_{cp}]$ of the centroid, as shown in Fig. 2, where the abscissa axis X_r represents the root cone of the tooth, O_r represents the apex of the root cone, and S_g represents the gear tooth surface.

2.2.1 Direction angle γ_{cp} of the contact pattern

The direction angle γ_{cp} is generally used to describe the distribution of the contact pattern on the tooth surface. In order to prevent defects such as outer diagonal contact, ill-shape contact, and no intersection of the adjacent TE curves, γ_{cp} is chosen as one of the description parameters. γ_{cp} is defined as the angle between the root cone of the tooth blank and the line connecting the points GT and GS (on the contact trajectory of the gear, the points where the teeth touch each other or separate from each other are respectively named GT and GS, which are the beginning and the end of the cycle of meshing for one pair of teeth (Litvin and Fuentes, 2004)), as shown in Fig. 3.

In some previous studies, such as the LSM (Wang and Ghosh, 1994; Litvin and Fuentes, 2004), the direction angle of the contact trajectory is generally defined as the angle between the root cone and the tangent line of the contact trajectory at the calculation point, as shown in Fig. 3. Actually, the tangential direction at the single point cannot determine the entire contact trajectory throughout the meshing process. The points on the contact trajectory but outside the curve from GS to GT are meaningless because at these points the mating surfaces have been separated from each other or have not yet touched each other. In this study, the calculation principle of γ_{cp} is redefined as

$$\gamma_{cp} = \arctan\left(\frac{y_{c_1} - y_{c_n}}{x_{c_1} - x_{c_n}}\right), \tag{1}$$

where $[x_{c_1}, y_{c_1}]$, $[x_{c_n}, y_{c_n}]$ are the coordinate values of GS(c_1) and GT(c_n), as shown in Figs. 2 and 3.

2.2.2 Area S_{cp} of the contact pattern

S_{cp} represents the area surrounded by the endpoints of all contact ellipses, which reflects the load bearing capacity of the gear pair, since a larger S_{cp} is more conducive to distributing the load and avoiding

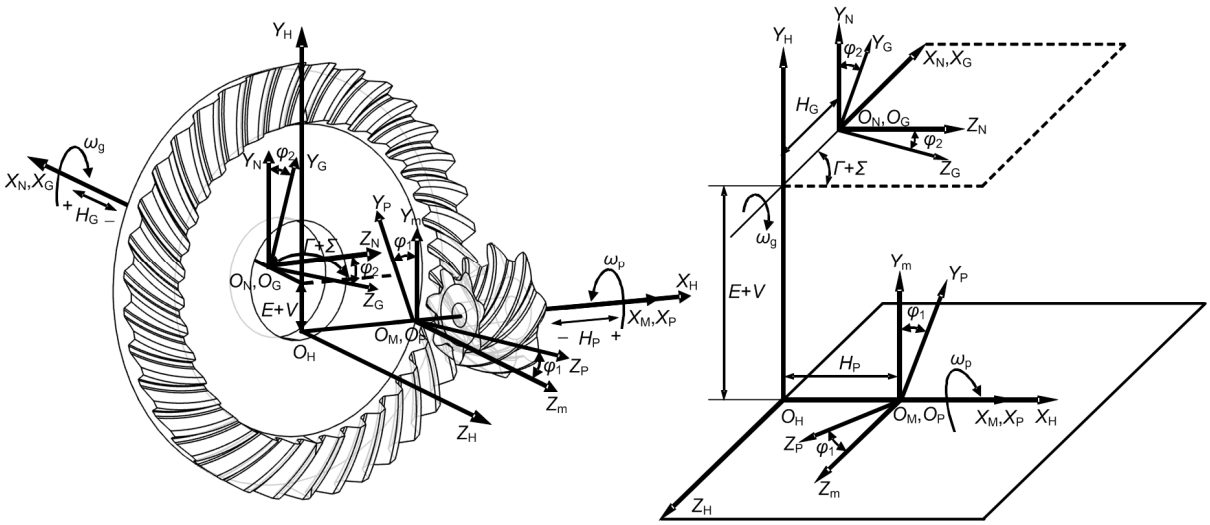

Fig. 1 Relative mounting errors of a hypoid gear pair

ω_g is the rotate speed of the gear; ω_p is the rotate speed of the pinion; other parameters are explained in the main text

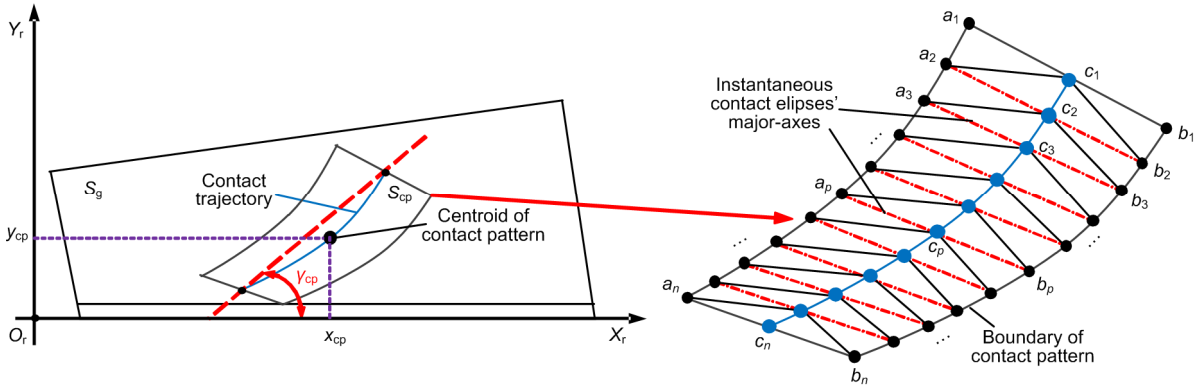

Fig. 2 Parametrization of the contact pattern on the gear surface

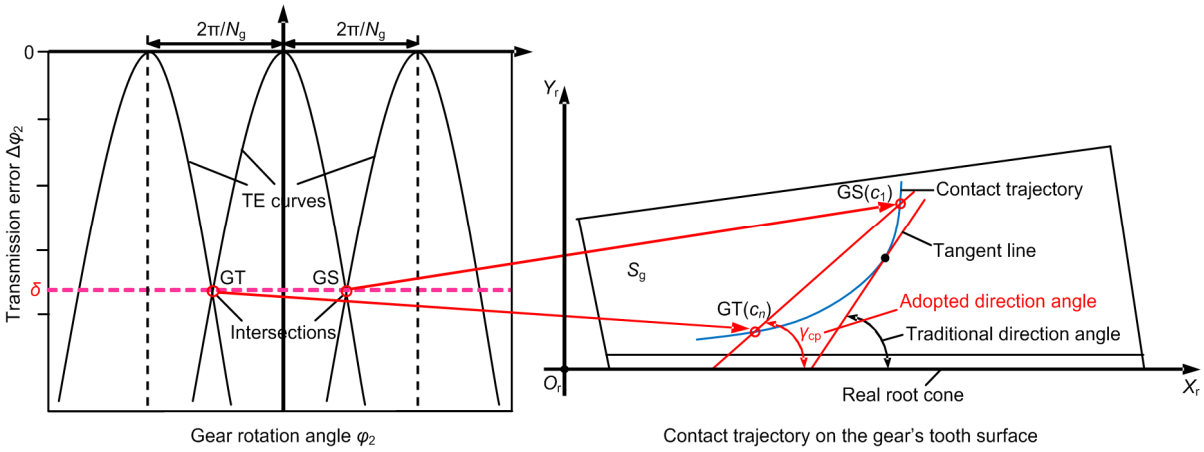

Fig. 3 Intersection of two adjacent TE curves and direction angle of the contact pattern

δ is the transmission error of the intersection of two adjacent TE curves

stress concentration. Because the boundaries of the contact pattern are all curved, in order to obtain S_{cp} accurately, the long boundaries of the contact pattern and the contact trajectory are respectively dispersed into n discrete points, as shown in Fig. 2. Therefore, the area S_{cp} can be calculated based on

$$S_{cp}=\sum_{p=1}^{n-1}\left[\frac{1}{2}\times\left(V_a+V_b+V_c\right)\right], \tag{2}$$

where n represents the number of points at which the left-side boundary, the right-side boundary, and the contact trajectory of the contact pattern are discretized during the TCA process. V_a, V_b, and V_c are the transition variables, and

$$V_a=\begin{vmatrix} x_{c_p} & y_{c_p} & 1\\ x_{a_p} & y_{a_p} & 1\\ x_{a_{(p+1)}} & y_{a_{(p+1)}} & 1\end{vmatrix},$$

$$V_b=\begin{vmatrix} x_{c_p} & y_{c_p} & 1\\ x_{a_{(p+1)}} & y_{a_{(p+1)}} & 1\\ x_{b_{(p+1)}} & y_{b_{(p+1)}} & 1\end{vmatrix},$$

$$V_c=\begin{vmatrix} x_{c_p} & y_{c_p} & 1\\ x_{b_p} & y_{b_p} & 1\\ x_{b_{(p+1)}} & y_{b_{(p+1)}} & 1\end{vmatrix}.$$

x_{a_p} and y_{a_p} represent the abscissa and the ordinate of the pth point on the left-side boundary of the contact point, respectively, and p=1, 2, …, n−1. x_{b_p} and y_{b_p} represent the abscissa and the ordinate of the pth point on the right-side boundary of the contact point, respectively. x_{c_p} and y_{c_p} represent the abscissa and the ordinate of the pth point on the contact trajectory of the contact point, respectively.

2.2.3 Coordinate $[\tilde{x}_{cp}, \tilde{y}_{cp}]$ of centroid of contact pattern

As shown in Fig. 2, the coordinate of the centroid of the contact pattern determines its position on the tooth surface, and coordinates can be calculated based on

$$\begin{aligned}\tilde{x}_{cp}=&\sum_{p=1}^{n-1}\left[\left(x_{c_p}+x_{a_p}+x_{a_{(p+1)}}\right)\cdot V_a\right.\\&+\left(x_{c_p}+x_{a_{(p+1)}}+x_{b_{(p+1)}}\right)\cdot V_b\\&\left.+\left(x_{c_p}+x_{b_p}+x_{b_{(p+1)}}\right)\cdot V_c\right]\\&\Big/\left[3\times\sum_{p=1}^{n-1}\left(V_a+V_b+V_c\right)\right],\\ \tilde{y}_{cp}=&\sum_{p=1}^{n-1}\left[\left(y_{c_p}+y_{a_p}+y_{a_{(p+1)}}\right)\cdot V_a\right.\\&+\left(y_{c_p}+y_{a_{(p+1)}}+y_{b_{(p+1)}}\right)\cdot V_b\\&\left.+\left(y_{c_p}+y_{b_p}+y_{b_{(p+1)}}\right)\cdot V_c\right]\\&\Big/\left[3\times\sum_{p=1}^{n-1}\left(V_a+V_b+V_c\right)\right].\end{aligned} \tag{3}$$

These parameters can accurately determine the direction, shape, and position of the contact pattern, to be used in the following sensitivity modeling as the evaluation parameters.

3 Modified TCA algorithm

The TCA algorithm considering alignment errors (AE-TCA) is a special tooth contact analysis approach that considers only installation errors, not machining errors. This is an effective method for studying the sensitivity and tolerance of misalignments. Before the tooth contact analysis, both the gear surface equations and the pinion surface equations should be formulated based on the tooth blank parameters, machine-tool settings, and the cutter parameters. The assembly coordinate system with mounting errors is shown in Fig. 1, where O_P and O_G are the predetermined origins of the pinion coordinate system and gear coordinate system, respectively. S_P (O_P, X_P, Y_P, Z_P) and S_G (O_G, X_G, Y_G, Z_G) are the coordinate systems fixed on the pinion and the gear, respectively. S_H (O_H, X_H, Y_H, Z_H) is the global assembly coordinate system. Γ and E are the ideal shaft angle and the offset between the pinion axis and the gear axis, respectively. S_M (O_M, X_M, Y_M, Z_M) and S_N (O_N, X_N, Y_N, Z_N) are the auxiliary calculating coordinate systems corresponding to the pinion and gear,

respectively. φ_1 and φ_2 are the real rotation angles of the pinion and gear, respectively.

On the pinion surface S_p and gear surface S_g, the radius vectors $\boldsymbol{r}_p$ and $\boldsymbol{r}_g$ and normal vectors $\boldsymbol{n}_p$ and $\boldsymbol{n}_g$ of S_P and S_G can be described as

$$\begin{cases} \boldsymbol{r}_p = \boldsymbol{r}_p(\theta_p, \phi_p), \\ \boldsymbol{r}_g = \boldsymbol{r}_g(\theta_g, \phi_g), \end{cases} \quad \begin{cases} \boldsymbol{n}_p = \boldsymbol{n}_p(\theta_p, \phi_p), \\ \boldsymbol{n}_g = \boldsymbol{n}_g(\theta_g, \phi_g), \end{cases} \tag{4}$$

where θ_p and θ_g represent the cutter rotation angles of the pinion and gear, respectively; ϕ_p and ϕ_g represent the work-piece rotation angles of the pinion and gear during the machining process, respectively.

Based on spatial coordinate transformation theory (Wu, 2009), the radius vectors $\boldsymbol{r}_H^p$ and $\boldsymbol{r}_H^g$ and normal vectors $\boldsymbol{n}_H^p$ and $\boldsymbol{n}_H^g$ in S_H can be represented as

$$\begin{cases} \boldsymbol{r}_H^p = \boldsymbol{M}_{HM}(H_P)\boldsymbol{M}_{MP}(\varphi_1)\boldsymbol{r}_p(\theta_p, \phi_p), \\ \boldsymbol{r}_H^g = \boldsymbol{M}_{HN}(H_G, E+V, \Gamma+\Sigma)\boldsymbol{M}_{NG}(\varphi_2)\boldsymbol{r}_g(\theta_g, \phi_g), \\ \boldsymbol{n}_H^p = \boldsymbol{L}_{HM}(H_P)\boldsymbol{L}_{MP}(\varphi_1)\boldsymbol{n}_p(\theta_p, \phi_p), \\ \boldsymbol{n}_H^g = \boldsymbol{L}_{HN}(H_G, E+V, \Gamma+\Sigma)\boldsymbol{L}_{NG}(\varphi_2)\boldsymbol{n}_g(\theta_g, \phi_g), \end{cases} \tag{5}$$

where $\boldsymbol{M}_{HM}$, $\boldsymbol{M}_{MP}$, $\boldsymbol{M}_{HN}$, and $\boldsymbol{M}_{NG}$ are the fourth-order homogeneous matrixes for transforming the calculating coordinate systems, which respectively represent the transformation matrix from S_M (O_M, X_M, Y_M, Z_M) to S_H (O_H, X_H, Y_H, Z_H), the transformation matrix from S_P (O_P, X_P, Y_P, Z_P) to S_M (O_M, X_M, Y_M, Z_M), the transformation matrix from S_N (O_N, X_N, Y_N, Z_N) to S_H (O_H, X_H, Y_H, Z_H), and the transformation matrix from S_G (O_G, X_G, Y_G, Z_G) to S_N (O_N, X_N, Y_N, Z_N). $\boldsymbol{L}_{HM}$, $\boldsymbol{L}_{MP}$, $\boldsymbol{L}_{HN}$, and $\boldsymbol{L}_{NG}$ are the matrixes corresponding to $\boldsymbol{M}_{HM}$, $\boldsymbol{M}_{MP}$, $\boldsymbol{M}_{HN}$, $\boldsymbol{M}_{NG}$ but the last rows and last columns are removed. $\boldsymbol{M}_{HN}(H_G, E+V, \Gamma+E)\boldsymbol{M}_{NG}(\varphi_2)$ can be expressed as

$$\boldsymbol{M}_{HN}(H_G, E+V, \Gamma+\Sigma)\,\boldsymbol{M}_{NG}(\varphi_2) = \begin{bmatrix} \cos(\Gamma+\Sigma) & \sin(\Gamma+\Sigma)\sin\varphi_2 & \sin(\Gamma+\Sigma)\cos\varphi_2 & -H_G\cos(\Gamma+\Sigma) \\ 0 & \cos\varphi_2 & -\sin\varphi_2 & E+V \\ -\sin(\Gamma+\Sigma) & \cos(\Gamma+\Sigma)\sin\varphi_2 & \cos(\Gamma+\Sigma)\cos\varphi_2 & H_G\sin(\Gamma+\Sigma) \\ 0 & 0 & 0 & 1 \end{bmatrix}, \tag{6}$$

and $\boldsymbol{M}_{HM}(H_P)\boldsymbol{M}_{MP}(\varphi_1)$ can be expressed as

$$\boldsymbol{M}_{HM}(H_P)\,\boldsymbol{M}_{MP}(\varphi_1) = \begin{bmatrix} 1 & 0 & 0 & H_P \\ 0 & \cos\varphi_1 & -\sin\varphi_1 & 0 \\ 0 & \sin\varphi_1 & \cos\varphi_1 & 0 \\ 0 & 0 & 0 & 1 \end{bmatrix}. \tag{7}$$

As shown in Fig. 4, based on the meshing theory of conjugate surfaces (Litvin et al., 1991), during the meshing process, the two conjugate surfaces are continuously point-contacting each other, and there is a tangent plane and a shared normal vector between the two surfaces, so the TCA equations considering installation errors can be expressed as

$$\begin{cases} \boldsymbol{r}_H^p(\theta_p, \phi_p, \varphi_1) = \boldsymbol{r}_H^g(\theta_g, \phi_g, \varphi_2), \\ \boldsymbol{n}_H^p(\theta_p, \phi_p, \varphi_1) = \boldsymbol{n}_H^g(\theta_g, \phi_g, \varphi_2), \\ \boldsymbol{n}_H^g \cdot \boldsymbol{V}_H^{pg} = 0, \end{cases} \tag{8}$$

where $\boldsymbol{V}_H^{pg}$ represents the relative speed vector at the contacting point of the surfaces of pinion and gear, which can be described as

$$\boldsymbol{V}_H^{pg} = (\omega_H^g - \omega_H^p) \times \boldsymbol{r}_H^g, \tag{9}$$

where ω_H^p and ω_H^g represent respectively the rotational angular velocities of the pinion and the gear during the meshing process, and can be defined as

$$\begin{cases} \omega_H^p = \begin{bmatrix} -1 & 0 & 0 \end{bmatrix}^T, \\ \omega_H^g = \dfrac{N_2}{N_1}\boldsymbol{M}_{HN}(H_G, E+V, \Gamma+\Sigma)\,\boldsymbol{M}_{NG}(\varphi_2)\begin{bmatrix} 1 & 0 & 0 \end{bmatrix}^T, \end{cases} \tag{10}$$

where N_1 and N_2 are the numbers of teeth of the pinion and the gear, respectively.

After projecting the radius vectors and normal vectors to the axes of the assembly coordinate system, the vector equations can be transformed to scalar equations, which contain six unknowns θ_p, ϕ_p, φ_1, θ_g, ϕ_g, and φ_2. Since $\boldsymbol{n}_H^p$ and $\boldsymbol{n}_H^g$ are unit vectors such that $\left|\boldsymbol{n}_H^p\right| = \left|\boldsymbol{n}_H^g\right| = 1$, the number of independent scalar equations is five. To solve the five equations, taking

φ_1 as an input variable, and leaving the other unknowns θ_p, ϕ_p, θ_g, ϕ_g, and φ_2 to be worked out afterwards, then the contact points on the surface of the pinion and of the gear will be obtained. Adjusting φ_1 to a specific step size and repeating the above calculation process until the current contact point is outside the effective boundaries of the surfaces, the path of the contact points can be obtained, and the transmission error of the gear drive is defined as

$$\Delta\varphi_2 = (\varphi_2 - \varphi_2^0) - \frac{N_1}{N_2}(\varphi_1 - \varphi_1^0), \tag{11}$$

where φ_1^0 and φ_2^0 are the initial rotation angles of the pinion and gear, respectively.

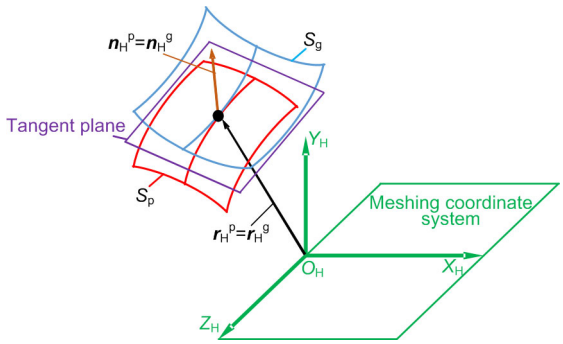

Fig. 4 Conjugate surfaces of a hypoid gear drive

For each instantaneous contact point, the cutting tool surface's principal directions and principal curvatures are known. Based on the curvature relation of two line-contact surfaces, the principal directions and principal curvatures of the surfaces of pinion and gear can be worked out. According to the curvature relation of two point-contact surfaces and considering the given elastic deformation d=0.00635 mm (Fan and Wilcox, 2007), the direction and dimensions of the contact ellipse can be calculated. All of the ellipses on the contact trajectory constitute the entire contact pattern. It should be noted that the unloaded TCA approach used in this study is a geometric contact analysis tool, which calculates the contact pattern and TE curve based on the gear geometry and the relative curvature parameters of the tooth surfaces. The influence of the relative sliding of the tooth surface is not considered.

4 Sensitivity analysis of contact patterns to installation errors

A face-hobbed hypoid gear pair is taken as the case for the sensitivity analysis of the contact pattern to alignment errors. The gear is processed by the generated method, and the pinion is processed by the cutter-tilted method. Basic geometric parameters of the example hypoid gears are given in Table 1. Referring to the settings of Litvin et al. (1995) and Simon (1998), variation ranges of the linear misalignments H_P, H_G, and V are set as [−0.3, +0.3] mm, and the variation range of the angular misalignment Σ is set as [−0.3°, +0.3°]. The change rules of γ_{cp}, S_{cp}, $\tilde{x}_{cp}$, and $\tilde{y}_{cp}$ are summarized in Fig. 5.

Angular misalignment Σ has the greatest influence on the direction angle, area, and position of the contact pattern. Besides Σ, the direction angle γ_{cp} is most sensitive to the offset misalignment V, while the area S_{cp} is most sensitive to the gear axial misalignment H_G. Position of the contact pattern on tooth length direction is most sensitive to the offset misalignment V, while the position of the contact pattern on tooth depth direction is most sensitive to the offset misalignment V and pinion axial misalignment H_P. The changes of the contact trajectories on the gear surface and pinion surface are shown in Fig. 6 (p.419). The offset misalignment V and the angular misalignment Σ have the greatest influence on the direction angle and the position of the contact pattern. The influence of the axial misalignment H_G of the gear is minimal, followed by the axial misalignment H_P of the pinion. Table 2 (p.419) gives a summary of the displacement trends of the contact patterns, which are the same as those obtained by Litvin et al. (1995). The change rules of the TE curves affected by the four misalignments are illustrated in Fig. 7 (p.420).

It can be observed from Fig. 7 that the influence of the axial misalignment of the gear, H_G, on the transmission stability is minimal, followed by the axial misalignment of the pinion, H_P. The running offset misalignment V and the angular misalignment Σ have the greatest influence on the transmission stability of the gear drive. These change rules verify the above conclusions of the impacts of misalignments on the contact trajectory and the evaluation

Table 1 Design data of the hypoid gear pair

Item	Description		Item	Description	
	Pinion (left-hand)	Gear (right-hand)		Pinion (active)	Gear
Number of teeth	7	36	Face angle (°)	17.57	77.28
Shaft angle (°)	90	90	Root angle (°)	12.37	71.97
Outer cone distance (mm)	197.29	185.04	Pitch apex beyond crossing point (mm)	12.17	−0.75
Offset (mm)	38	38	Face cone apex beyond crossing point (mm)	4.41	−1.06
Tooth width (mm)	54.22	48.00	Root cone apex beyond crossing point (mm)	4.73	−0.66
Mean spiral angle (°)	50.00	36.38	Mean addendum (mm)	12.87	1.93
Pressure angle (°)	22.5	–	Mean dedendum (mm)	4.22	14.85
Pitch angle (°)	13.0	76.6	Working depth (mm)	14.84	14.84
Tool fillet radius (mm)	1.4 (convex) 1.4 (concave)	3.2	Tool nose radius (mm)	162.0 (convex) 141.0 (concave)	152.4

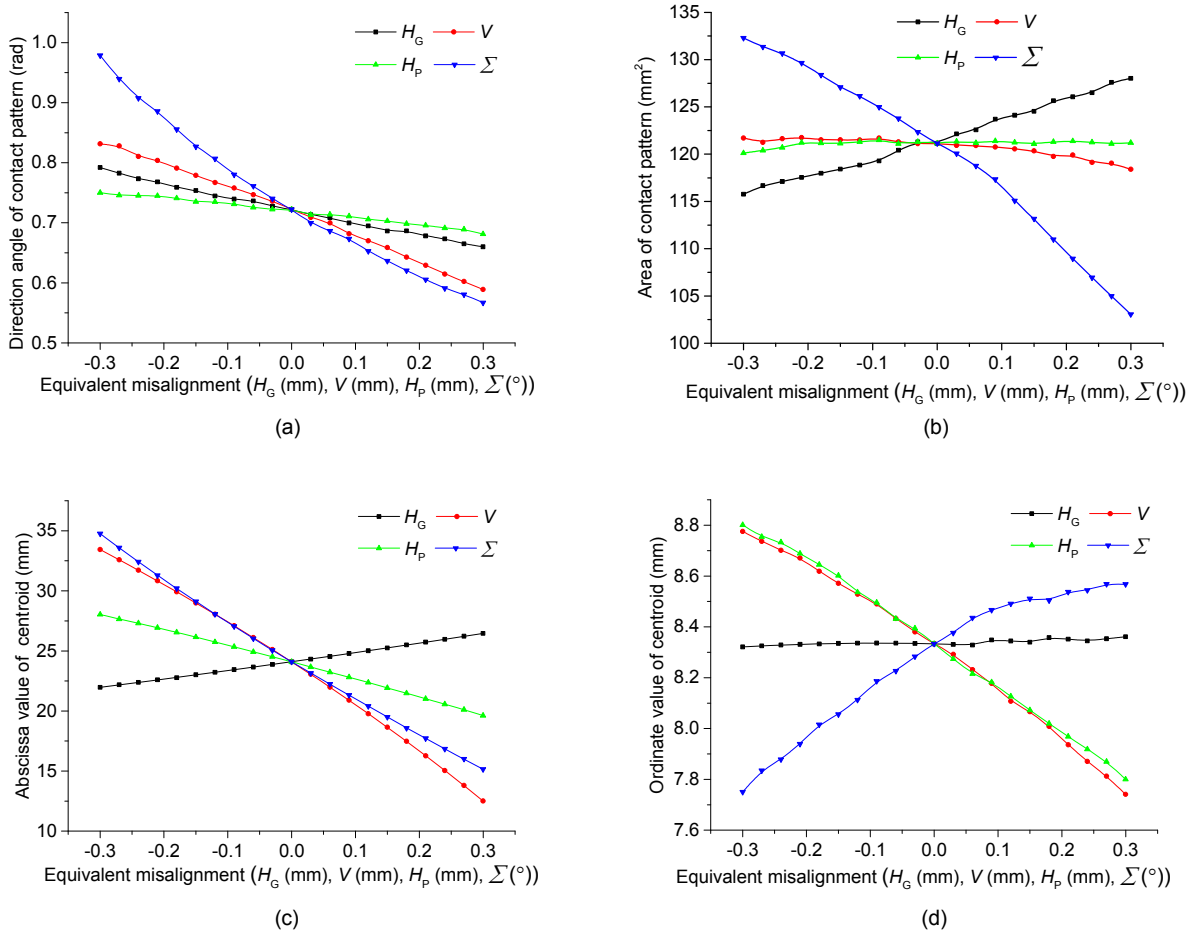

Fig. 5 Change rules of evaluation indexes of contact pattern

(a) Direction angle of contact pattern, γ_{cp}; (b) Area of contact pattern, S_{cp}; (c) Abscissa value of contact pattern's centroid, $\tilde{x}_{cp}$; (d) Ordinate value of contact pattern's centroid, $\tilde{y}_{cp}$

parameters of the contact pattern, which provide the basis of the following optimization process.

Table 2 Shift of contact trajectory due to misalignments

Misalignment	Shift on gear	Shift on pinion
H_G (+)	Heel and low	Heel and high
H_G (−)	Toe and high	Toe and low
V (+)	Toe and high	Toe and low
V (−)	Heel and low	Heel and high
H_P (+)	Toe and high	Toe and low
H_P (−)	Heel and low	Heel and high
Σ (+)	Toe and high	Toe and low
Σ (−)	Heel and low	Heel and high

5 Sensitivity optimization design

To improve the meshing performance and the stability of the gear drive, the centroid of the contact pattern should be located in the middle of the tooth surface and the area should be appropriately larger to optimize the load distribution (Zeng, 1989). The effective overlap ratio (EOR) can reflect the number of simultaneously meshing tooth pairs. In a reasonable range, the EOR will increase with the decrease of γ_{cp} (Zeng, 1989), and a higher EOR can enhance the gear pair's bearing capacity and reduce meshing vibration (Deng and Wei, 2012). Therefore, the

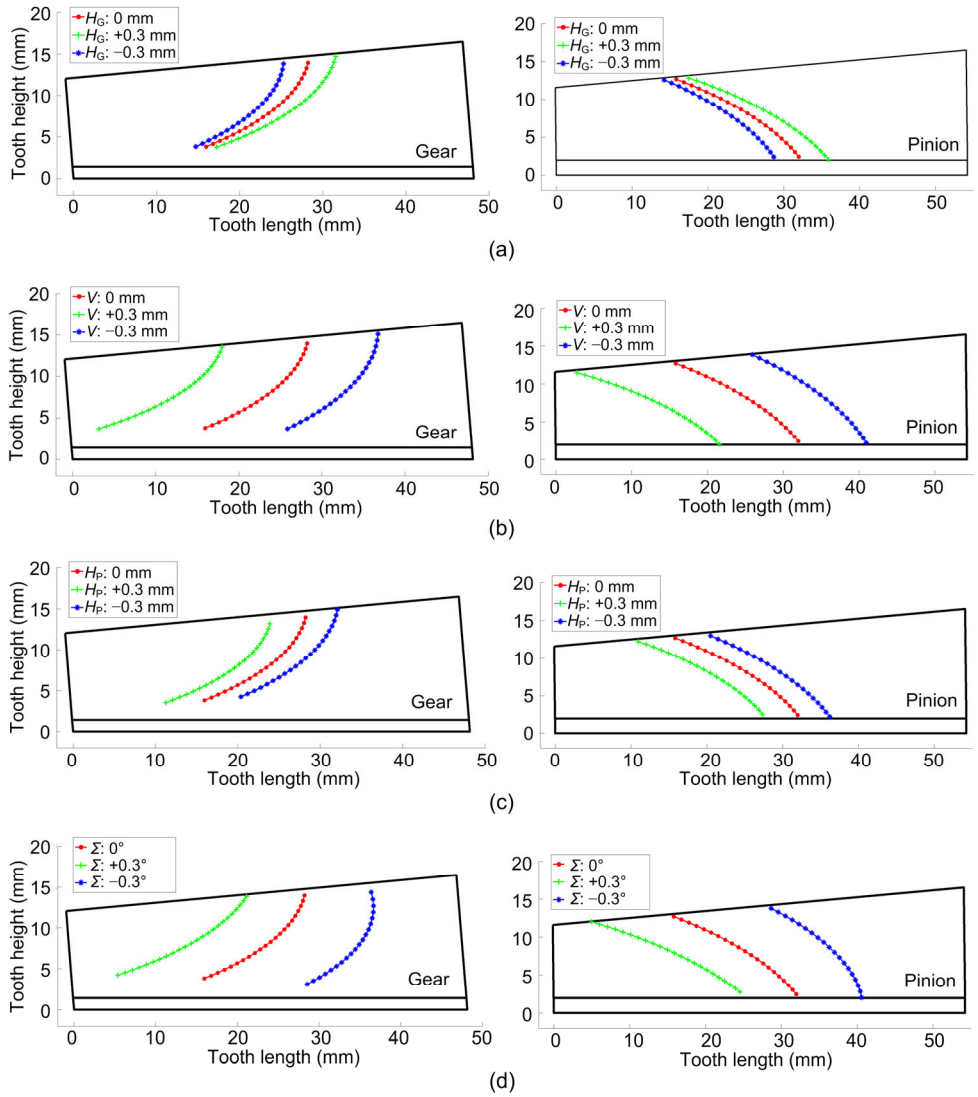

Fig. 6 Impacts of the installation errors on the contact trajectory on the gear and pinion surfaces
(a) H_G: ±0.3 mm; (b) V: ±0.3 mm; (c) H_P: ±0.3 mm; (d) Σ: ±0.3°

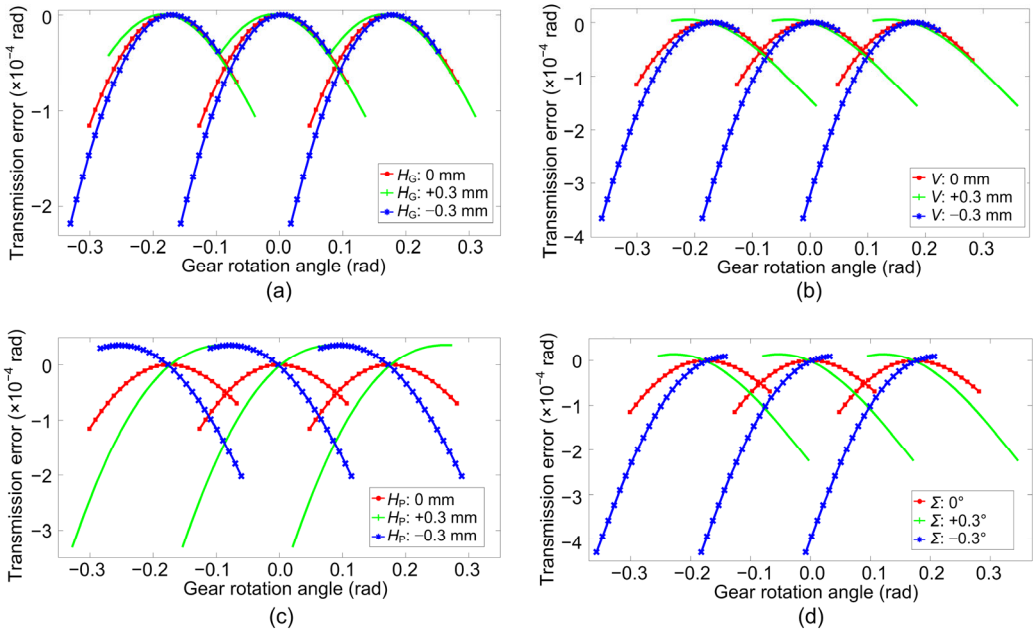

Fig. 7 Change rules of transmission error affected by the four misalignments
(a) H_G: ±0.3 mm; (b) V: ±0.3 mm; (c) H_P: ±0.3 mm; (d) Σ: ±0.3°

direction angle γ_{cp} should be controlled within a reasonable range.

5.1 Sensitivity model of contact pattern

Taking γ_{cp}, S_{cp}, $\tilde{x}_{cp}$, and $\tilde{y}_{cp}$ obtained in the state without installation errors as the theoretical parameters, the contact pattern errors are defined as the differences between the theoretical values and the actual values of the four parameters. $\Delta\tilde{x}_{cp}$, $\Delta\tilde{y}_{cp}$, ΔS_{cp}, $\Delta\gamma_{cp}$ represent the centroid's horizontal and vertical position errors, and the area and the direction angle errors of the contact pattern, respectively, and can be described as

$$\begin{cases}\Delta\tilde{x}_{cp}=f_x(H_P,H_G,V,\Sigma),\\ \Delta\tilde{y}_{cp}=f_y(H_P,H_G,V,\Sigma),\\ \Delta S_{cp}=f_s(H_P,H_G,V,\Sigma),\\ \Delta\gamma_{cp}=f_\gamma(H_P,H_G,V,\Sigma).\end{cases} \tag{12}$$

The sensitivities of the contact pattern to installation errors are defined as the changing rate of the four description parameters H_P, H_G, V, and Σ relative to equivalent misalignments $\Delta\tilde{x}_{cp}$, $\Delta\tilde{y}_{cp}$, ΔS_{cp}, and $\Delta\gamma_{cp}$. The larger the absolute value, the more sensitive the parameter will be, which can be represented as

$$\begin{cases}\boldsymbol{S}_x=\nabla f_x=\left[\dfrac{\partial f_x}{\partial H_P},\dfrac{\partial f_x}{\partial H_G},\dfrac{\partial f_x}{\partial V},\dfrac{\partial f_x}{\partial\Sigma}\right]^{\mathrm{T}},\\ \boldsymbol{S}_y=\nabla f_y=\left[\dfrac{\partial f_y}{\partial H_P},\dfrac{\partial f_y}{\partial H_G},\dfrac{\partial f_y}{\partial V},\dfrac{\partial f_y}{\partial\Sigma}\right]^{\mathrm{T}},\\ \boldsymbol{S}_s=\nabla f_s=\left[\dfrac{\partial f_s}{\partial H_P},\dfrac{\partial f_s}{\partial H_G},\dfrac{\partial f_s}{\partial V},\dfrac{\partial f_s}{\partial\Sigma}\right]^{\mathrm{T}},\\ \boldsymbol{S}_\gamma=\nabla f_\gamma=\left[\dfrac{\partial f_\gamma}{\partial H_P},\dfrac{\partial f_\gamma}{\partial H_G},\dfrac{\partial f_\gamma}{\partial V},\dfrac{\partial f_\gamma}{\partial\Sigma}\right]^{\mathrm{T}}.\end{cases} \tag{13}$$

5.2 Multi-objective function of sensitivity

Considering the comprehensive effects of these four kinds of misalignments, the sensitivity optimization problem of the contact pattern is actually a multi-objective problem, which can be represented as

$$\left\{\min\sum_{i=1}^{4}\left|S_{x_i}\right|,\min\sum_{i=1}^{4}\left|S_{y_i}\right|,\min\sum_{i=1}^{4}\left|S_{s_i}\right|,\min\sum_{i=1}^{4}\left|S_{\gamma_i}\right|\right\}. \tag{14}$$

Eq. (14) represents the minimum misalignment sensitivity for each of the above four indicators. In order to translate the multi-objective function to a single-objective function, the four sub-functions are weighted based on the conclusions of the above sensitivity analysis. After weighting the four goals, the multi-objective function can be described as

$$\min f(d_j)=C_1\sum_{i=1}^{4}\left|S_{x_i}\right|+C_2\sum_{i=1}^{4}\left|S_{y_i}\right|+C_3\sum_{i=1}^{4}\left|S_{s_i}\right|+C_4\sum_{i=1}^{4}\left|S_{\gamma_i}\right|,$$
$$C_1+C_2+C_3+C_4=1, \tag{15}$$

where d_j represents the optimization control variables, and C_i (i=1, 2, 3, 4) represents the weighting coefficients for the four sub-objective functions, which can be determined based on the conclusion of the above sensitivity analysis and the assembly and bearing requirements in practice. It can be seen from Figs. 5 and 6 that the horizontal position and the area of the contact pattern are more sensitive than the vertical position and the direction angle, so in the following study, C_1 and C_3 will be set larger than C_2 and C_4.

5.3 Optimization process

According to the conjugate contact theory and gear meshing principle (Litvin and Fuentes, 2004), the induced normal curvatures and induced geodesic torsion jointly determine the meshing features (Zeng, 1989). In both LCT and LSM, firstly, the gear surface S_g must be derived based on the tooth blank parameters, machine-tool settings, and the cutter parameters (Zeng, 1989; Litvin and Fuentes, 2004). The convex and concave surfaces of the gear are all determined, and thus contact properties only depend on the curvatures of the pinion surfaces. The essence of LCT and LSM is to adjust the induced normal curvatures and induced geodesic torsion between the contacting surfaces by adjusting the curvatures of the pinion.

As shown in Fig. 8, the curvatures A_g, B_g, and C_g of the gear surface at the calculation point can be computed based on the line-contact conjugate theory (Wu, 2009). Based on the line conjugate contact theory, three induced curvatures ΔA_{pg}, ΔB_{pg}, and ΔC_{pg} between the imaginary pinion and the gear can be calculated. By calculating the difference between A_g, B_g, C_g and ΔA_{pg}, ΔB_{pg}, ΔC_{pg}, the curvatures A_{pl}, B_{pl}, and C_{pl} of the design pitch cone of the imaginary pinion can be obtained, which is line-contacting with the gear. In LCT, the gear designer will calculate the curvature correction values ΔA, ΔB, and ΔC based on A_{pl}, B_{pl}, and C_{pl} to turn the contact state from the fully conjugate line-contact to the locally conjugate point-contact. Then the curvatures A_p, B_p, and C_p of the design pitch cone of the pinion can be obtained based on ΔA, ΔB, ΔC and A_{pl}, B_{pl}, C_{pl}, which is point-contacting with the gear.

In this methodology, after getting the curvatures A_p, B_p, and C_p of the pinion surface by LCT, the target scope of A_p, B_p, and C_p is set to a predetermined range $\boldsymbol{A}_p^{\mathrm{T}}$, $\boldsymbol{B}_p^{\mathrm{T}}$, and $\boldsymbol{C}_p^{\mathrm{T}}$ based on the initially obtained value of A_p, B_p, C_p, which can be obtained based on

$$\begin{cases}\boldsymbol{A}_p^{\mathrm{T}}=[(1-a_p)A_p,\ (1+a_p)A_p],\\ \boldsymbol{B}_p^{\mathrm{T}}=[(1-b_p)B_p,\ (1+b_p)B_p],\\ \boldsymbol{C}_p^{\mathrm{T}}=[(1-c_p)C_p,\ (1+c_p)C_p],\end{cases} \tag{16}$$

where a_p, b_p, c_p are the scaling factors of A_p, B_p, C_p, respectively, which should be determined by the actual case of the gear pair and generally set as 0.05 to 0.1. After the new range is established, the initial individual $\boldsymbol{X}^k=[A_p^k, B_p^k, C_p^k]^{\mathrm{T}}$ (k=1, 2, …, M_p) of A_p, B_p, C_p will be generated by the M_p individuals randomly selected from $\boldsymbol{A}_p^{\mathrm{T}}$, $\boldsymbol{B}_p^{\mathrm{T}}$, $\boldsymbol{C}_p^{\mathrm{T}}$, where M_p is the preset number of the individuals. To avoid interference between the gear and pinion surfaces, each new set of A_p, B_p, and C_p in $\boldsymbol{X}^k$ must satisfy

$$\Delta A=A_p-A_{pl},\ \Delta B=B_p-B_{pl},\ \Delta C=C_p-C_{pl},$$
$$\Delta A\Delta B-(\Delta C)^2\geq 0. \tag{17}$$

The initial set of A_p, B_p, C_p and the global selection space of the curvatures of the pinion are illustrated in Fig. 9. The design pitch cone and the generating pitch cone of the pinion are not collinear, and the angle Δ between them can be calculated from (Zeng, 1989)

$$\sin\Delta=(\boldsymbol{T}_p,\ \boldsymbol{T}_{p'},\ \boldsymbol{N}_p),$$
$$\cos\Delta=\boldsymbol{T}_p\cdot\boldsymbol{T}_{p'}, \tag{18}$$

where $\boldsymbol{T}_p$ and $\boldsymbol{T}_{p'}$ represent the unit vectors along the tooth trace directions of the design pitch cone and generating cone, respectively, and $\boldsymbol{N}_p$ represents the unit normal vector of the pinion surface.

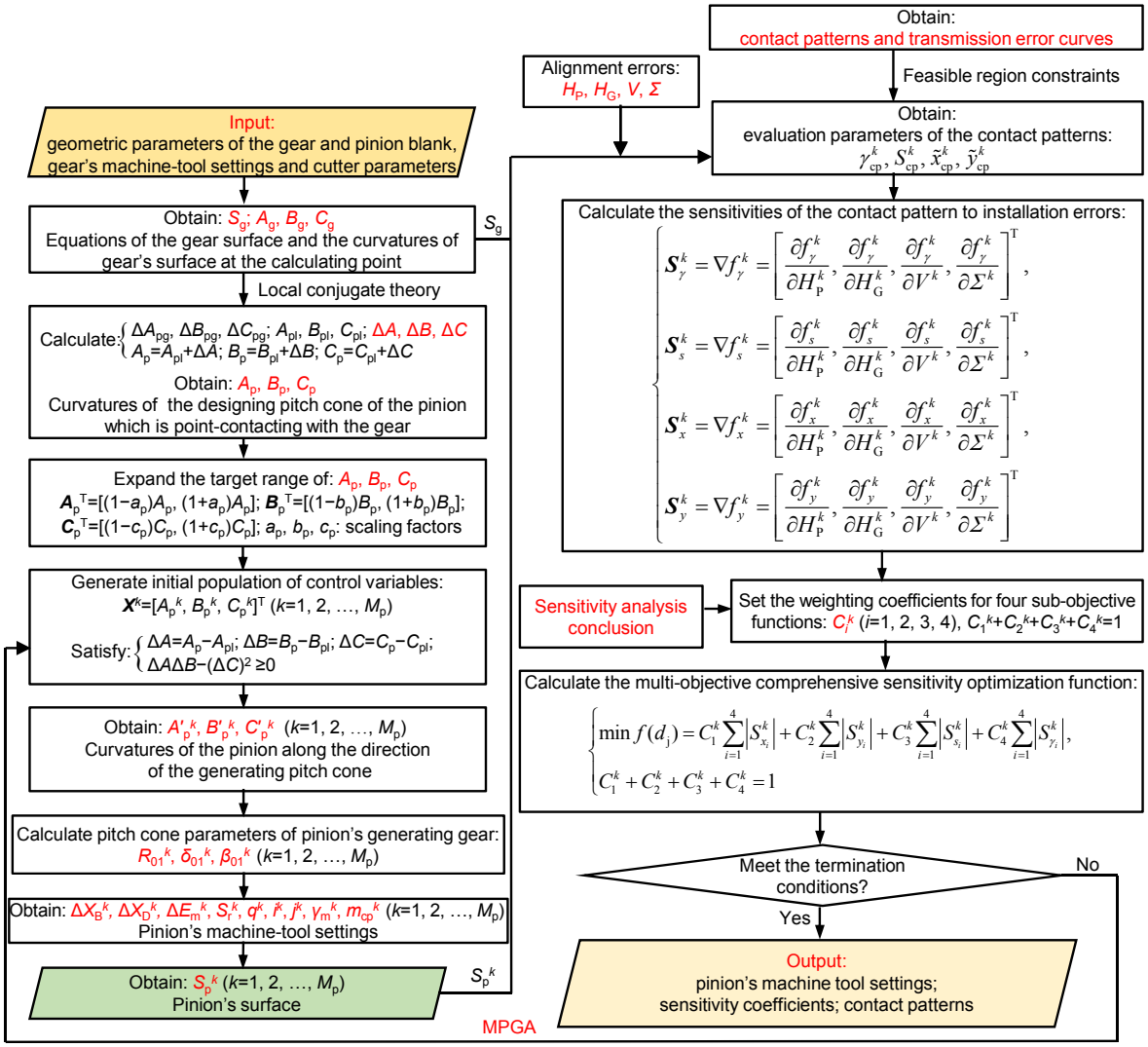

Fig. 8 Flowchart of the optimization process (MPGA is multi-population genetic algorithm)

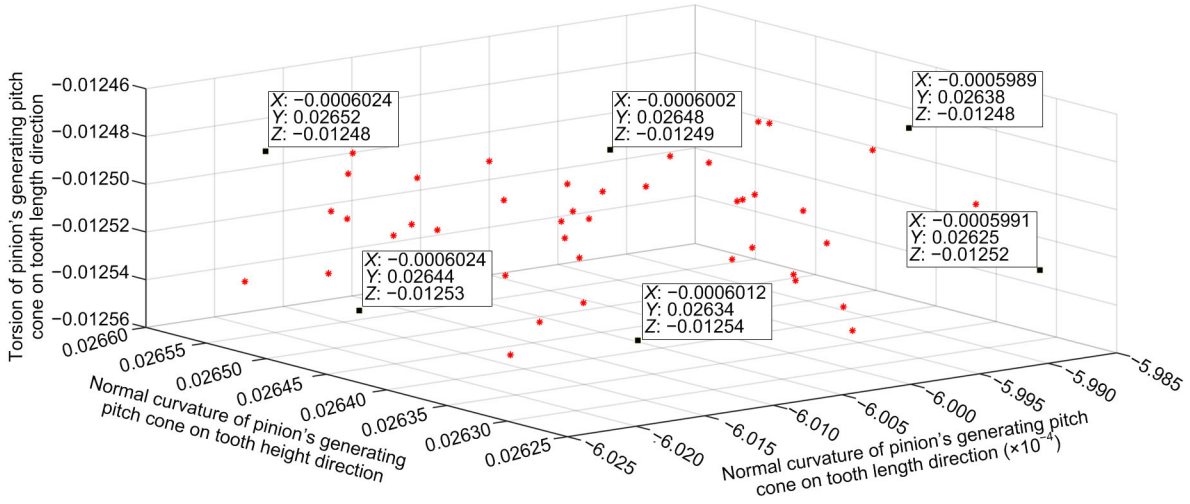

Fig. 9 Global selection space of the curvature of the pinion

For each individual in $\boldsymbol{X}^k$, the curvatures $A_p'^k$, $B_p'^k$, $C_p'^k$ of the pinion along the direction of the generating pitch cone can be computed based on the Euler and Bertrand formulas (Zeng, 1989).

$$\begin{aligned} A_p' &= A_p\cos^2\Delta + B_p\sin^2\Delta - 2C_p\sin\Delta\cos\Delta,\\ B_p' &= A_p\sin^2\Delta + B_p\cos^2\Delta + 2C_p\sin\Delta\cos\Delta,\\ C_p' &= (A_p - B_p)\sin\Delta\cos\Delta + C_p(\cos^2\Delta - \sin^2\Delta). \end{aligned} \tag{19}$$

According to $A_p'^k$, $B_p'^k$, $C_p'^k$ and the geometric parameters of the gear pair, the machining radius $r_M{}^k$ of the cutter head of pinion can be calculated, and the formulas are those in (Zeng, 1989). Then the parameters of the pitch cone of the generating gear of the pinion, such as the pitch cone distance $R_{01}{}^k$, pitch cone angle $\delta_{01}{}^k$, and the helical angle $\beta_{01}{}^k$, can be obtained (Zeng, 1989). Based on the tooth blank parameters and geometric parameters of the pinion and the pitch cone parameters of its generating gear, the machine-tool settings $\Delta X_B{}^k$, $\Delta X_D{}^k$, $\Delta E_m{}^k$, $S_r{}^k$, q^k, i^k, j^k, $\gamma_m{}^k$, $m_{cp}{}^k$ can be calculated (Zeng, 1989), as shown in Fig. 10 and Table 3.

The coordinate systems S_{ml} (O_{ml}, X_{ml}, Y_{ml}, Z_{ml}), S_q (O_q, X_q, Y_q, Z_q), S_1 (O_1, X_1, Y_1, Z_1), S_c (O_c, X_c, Y_c, Z_c), S_{tl} (O_{tl}, X_{tl}, Y_{tl}, Z_{tl}) are respectively fixed to the machine-tool, the work-piece stage, the pinion work-piece, cradle, and cutter. The cutting ratio m_{cp} is also an adjustable machine-tool parameter which is defined as

$$m_{cp} = \frac{\omega_c}{\omega_w}, \tag{20}$$

where ω_c and ω_w are the rotate speeds of the cradle and work-piece, respectively.

Based on the obtained machine-tool settings, tooth blank parameters and cutter parameters of the pinion, the equations of the pinion surfaces $S_p{}^k$ can be deduced. After that the gear and the pinion are assembled in the meshing coordinate system with four installation errors H_P, H_G, V, Σ. The AE-TCA between the gear surface S_g and the pinion surfaces $S_p{}^k$ considering misalignments, can be performed, then the evaluation parameters $\gamma_{cp}{}^k$, $S_{cp}{}^k$, $x_{cp}{}^k$, $y_{cp}{}^k$ of the contact patterns can be obtained. Based on these evaluation parameters, the sensitivities S_γ^k, S_s^k, S_x^k, S_y^k of the contact pattern to four installation errors can be worked out. According to the sensitivity analysis, the weighting coefficients C_i^k (i=1, 2, 3, 4) for four sub-objective functions corresponding to four evaluation parameters can be determined. The comprehensive sensitivity between S_g and the pinion surface $S_p{}^k$ corresponding to each individual in the generation can be calculated. Then, the minimum of the comprehensive sensitivities of this generation is obtained. Before reaching the termination condition, the above calculation will be performed iteratively by using a genetic algorithm (GA). The machine-tool settings of the pinion are continuously updated, and

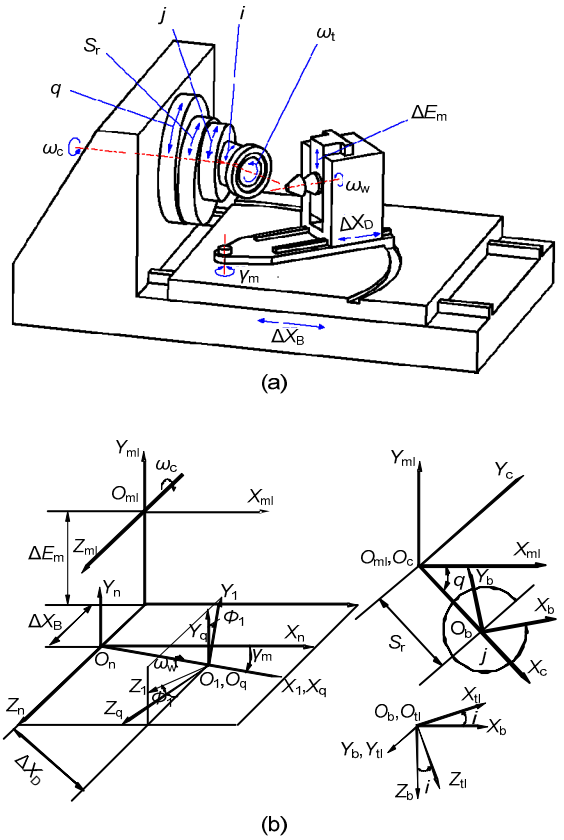

Fig. 10 Cradle-type generator model
(a) Machine-tool model; (b) Machining coordinate system

Table 3 Motion elements of the cradle-type generator

Item	Related motion	Item	Related motion
i	Tilt angle	ΔE_m	Blank offset
j	Swivel angle	ΔX_B	Sliding base
q	Basic cradle angle	ΔX_D	Machine center to back
S_r	Radial setting	γ_m	Machine root angle

consequently the pinion surface S_p^k is also updated. Finally, the individual with the minimal sensitivity is calculated, and thus the machine-tool settings and the tooth surface S_p^k can be obtained.

5.4 Constraints

In order to avoid the edge and corner contact states, the distribution of the contact pattern should be limited within a reasonable range on the tooth surface. As described in (Zeng, 1989; Wang et al., 2018), compared with the unloaded meshing state, the boundaries of the contact pattern under the loaded state will extend towards the edges of the tooth surface. Therefore, in the unloaded condition, the edges of the feasible region of the contact pattern should move a certain distance inward from the actual edge, as illustrated in Fig. 11.

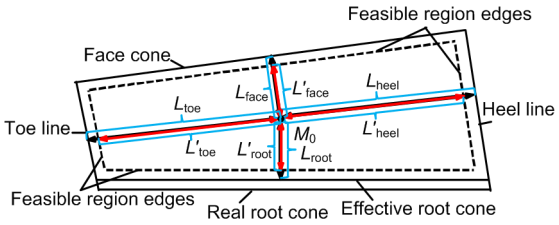

Fig. 11 Feasible region of the contact pattern

The distances between the calculating point M_0 and the face cone, effective root cone, toe line, and heel line are named L_{face}, L_{root}, L_{toe}, and L_{heel}, respectively. Similarly, the distances between M_0 and the corresponding edges of the feasible region are named L'_{face}, L'_{root}, L'_{toe}, and L'_{heel}. A shrinkage ratio of the four directions has been used to define the feasible region, which can be represented as

$$i_D = L'_D / L_D, \tag{21}$$

where the subscript D represents the face, root, toe, or heel. As described in (ANSI-AGMA, 2005), i_D is generally set in the range from 0.85 to 0.95. As shown in Fig. 12, assuming the new regions on the gear and pinion surfaces are S_g^* and S_p^*, respectively, if there is a real contacting point P_0 on these regions (Fig. 12a), the following expressions can be derived:

$$\begin{cases} S_g^{face} + S_g^{root} + S_g^{toe} + S_g^{heel} = S_g^*, \\ S_p^{face} + S_p^{root} + S_p^{toe} + S_p^{heel} = S_p^*, \end{cases} \tag{22}$$

where S_g^{face}, S_g^{root}, S_g^{toe}, S_g^{heel} are the triangular areas respectively formed by the contacting point P_0 with the new edges corresponding to the face cone, root cone, toe line, and heel line. If P_0 is outside the constrained area (Fig. 12b), the following expressions can be derived:

$$\begin{cases} S_g^{face} + S_g^{root} + S_g^{toe} + S_g^{heel} > S_g^*, \\ S_p^{face} + S_p^{root} + S_p^{toe} + S_p^{heel} > S_p^*. \end{cases} \tag{23}$$

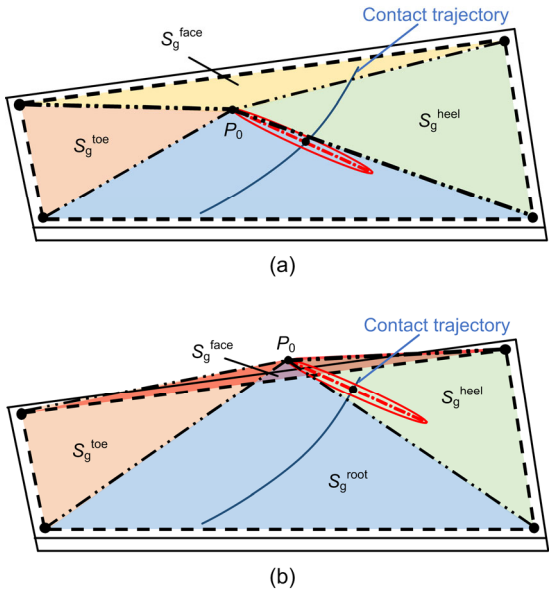

Fig. 12 Feasible region of the contact pattern
(a) Reasonable contact point; (b) False contact point

5.5 Constraint strategy of feasible region

In previous studies, for the convenience of computation, the researchers have usually limited the contact trajectory rather than use the entire contact pattern to control the meshing properties. In fact, the contact pattern consists of the instantaneous contact ellipses, so the length of each ellipse's long axis must be considered in the design of the pattern of the feasible region of contact. Furthermore, the curves below the intersection of two adjacent TE curves are meaningless because these curves correspond to the states in which the gear and pinion have separated from each other or not yet touched each other. The constraint strategy in this study can be summarized as shown in Fig. 13.

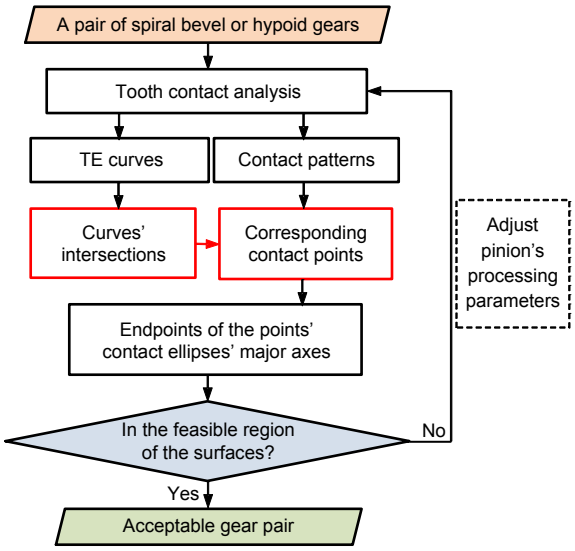

Fig. 13 Constraint strategy of feasible region

6 Optimization algorithm

With the rise of intelligent algorithms, more and more engineering problems have been successfully solved by heuristic optimization approaches, including the GA. GA is a nature-inspired stochastic optimization method which is suitable for solving complex technical problems. However, few studies have used intelligent algorithms for the optimum research of spiral bevel and hypoid gears.

As mentioned above, the multi-objective function is established based on TCA results after virtual machining and virtual assembly processes. This makes it a complex nonlinear problem. Due to the limitations of local convergence and premature convergence, GA generally cannot find the optimal result of such a strong nonlinear problem. In the last few years, a multi-population genetic algorithm (MPGA) has been proposed to eliminate the defects of GA (Pourvaziri and Naderi, 2014) as shown in Fig. 14.

The variation scopes of the curvatures are all constrained within a tiny range, while the new individuals have a certain degree of randomness, which may make the optimal solution of the offspring population not as good as that for the parental population. Considering the complexity of the multi-objective function, these factors will reduce the calculation speed. The cooperative operation of the elitism strategy and population catastrophe strategy has been introduced into this algorithm, as shown in Fig. 14. The elitism strategy means the best solution of parental population must be retained to the offspring population. Population catastrophe strategy means that when the average fitness value of the current population is close to the optimal fitness value, the mutation rate of the offspring population should be artificially improved.

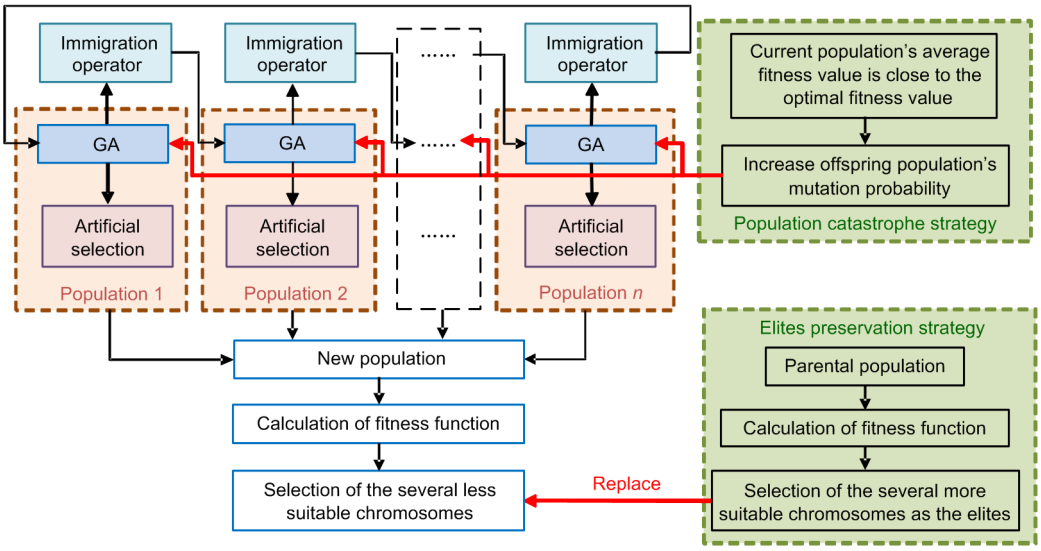

Fig. 14 MPGA with elitism preservation and population catastrophe cooperative strategy

7 Case study

A hypoid gear pair (the gear is processed by the generating method, and the pinion is processed by the cutter tilting method) is chosen to verify the feasibility of this method. The basic geometric parameters and cutting tool parameters of the example gear pair are given in Table 1, the convex surface of the gear and the concave surface of the pinion are the working surface of the gear drive, which have been chosen as case studies. The four equivalent misalignments are shown in Table 4, and the original contact patterns and transmission error curves are shown in Fig. 15.

Table 4 Equivalent misalignments

H_G (mm)	H_P (mm)	V (mm)	Σ (°)
0.173 17	0.118 27	0.108 51	0.101 19

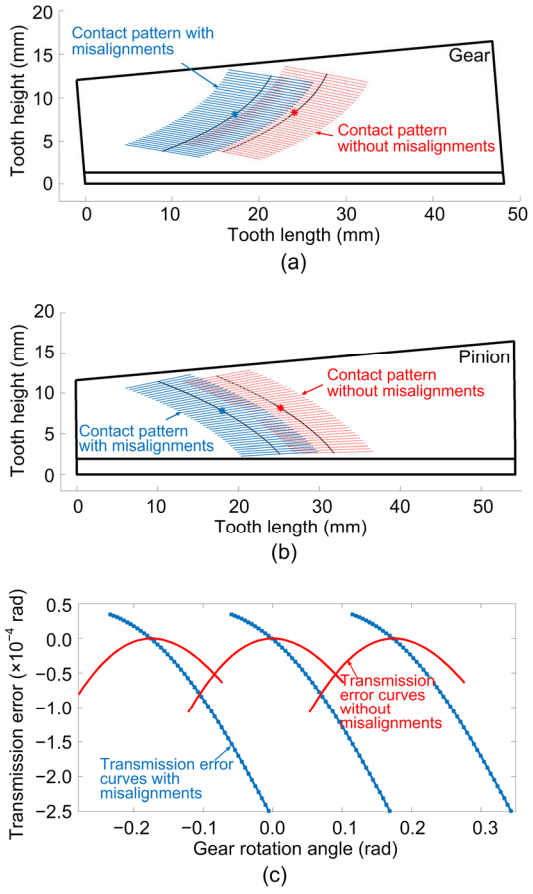

Fig. 15 Contact patterns on gear (a) and pinion (b) and TE curves (c) of the original hypoid gear pair

The evaluation parameters of the contact pattern without consideration of misalignments are given in Table 5, while the evaluation parameters considering misalignments are given in Table 6. Table 7 lists the sensitivity coefficients of the evaluation parameters to the four misalignments. The absolute value of each value represents the magnitude of sensitivity, and the greater the absolute value the more sensitive it is.

Table 5 Evaluation indexes of contact pattern without consideration of misalignments before optimization

γ_{cp} (rad)	S_{cp} (mm^2)	x_{cp} (mm)	y_{cp} (mm)
0.7223	122.4336	24.0653	8.3093

Table 6 Evaluation indexes of contact pattern with consideration of misalignments before optimization

γ_{cp} (rad)	S_{cp} (mm^2)	x_{cp} (mm)	y_{cp} (mm)
0.6451	111.2434	12.0978	7.8717

Table 7 Sensitivity coefficients of the original design

Misalignment	S_γ	S_s	S_x	S_y
H_G	−0.226 91	20.417 17	7.478 48	0.066 38
H_P	−0.115 09	1.809 70	−14.027 63	−1.668 58
V	−0.404 27	−5.512 27	−34.902 04	−1.724 28
Σ	−0.686 23	−48.724 25	−32.685 70	1.362 44

According to the above sensitivity analysis conclusion, the weighting coefficients C_i^k (i=1, 2, 3, 4) in this case can be set as

$$C_1 = C_3 = 0.35,\ C_2 = 0.1,\ C_4 = 0.2. \tag{24}$$

Parameters of each operator in the adopted MGPA optimization algorithm are given in Table 8. After completing the above-mentioned sensitivity optimization and the tooth contact analysis, the contact patterns and TE curves of the mating surfaces are shown in Fig. 16. Evaluation parameters of the contact pattern without the consideration of misalignments are listed in Table 9, while those with the consideration of misalignments are given in Table 10.

The sensitivity coefficients obtained after optimization are shown in Table 11. The values in parentheses indicate the changes in the absolute value of the sensitivity coefficient. A positive value indicates

an increased sensitivity and a negative value indicates a decreased sensitivity.

Table 8 Parameters of MPGA optimization algorithm

Number of iterations	Number of individuals	Number of subpopulations	Crossover probability
100	40	4	0.8
Mutation probability	**Migration probability**	**Generation gap**	**Migration cycle**
0.3	0.3	0.8	3

Table 9 Evaluation indexes of contact pattern without consideration of misalignments after optimization

γ_{cp} (rad)	S_{cp} (mm^2)	x_{cp} (mm)	y_{cp} (mm)
0.7036	141.2345	23.744	8.0772

Table 10 Evaluation indexes of contact pattern with consideration of misalignments after optimization

γ_{cp} (rad)	S_{cp} (mm^2)	x_{cp} (mm)	y_{cp} (mm)
0.6794	135.0937	20.3356	8.5710

It can be seen from Figs. 15 and 16 that the optimized contact patterns on the surfaces of the gear and pinion become less sensitive to the misalignments. Although the absolute value of the intersection of the TE curves becomes larger after optimization, it is still within a reasonable and acceptable range, which is generally set as [0.004°, 0.010°] (Simon, 1998). More importantly, the shapes of the optimized TE curves become more reasonable, whether or not the misalignments are considered. Undoubtedly, a transmission error curve with a parabolic shape is necessary for the desired meshing performance (Litvin and Fuentes, 2004). It can be observed from Table 11 that most sensitivities have decreased after the optimization. The sensitivities of the vertical position of the centroid to the gear's axial error, the offset error, and the angular error have increased respectively. The sensitivities of the direction angle and the area to the offset error have also increased. However, the other 11 sensitivities have been reduced, and the comprehensive sensitivity of the contact patterns to the

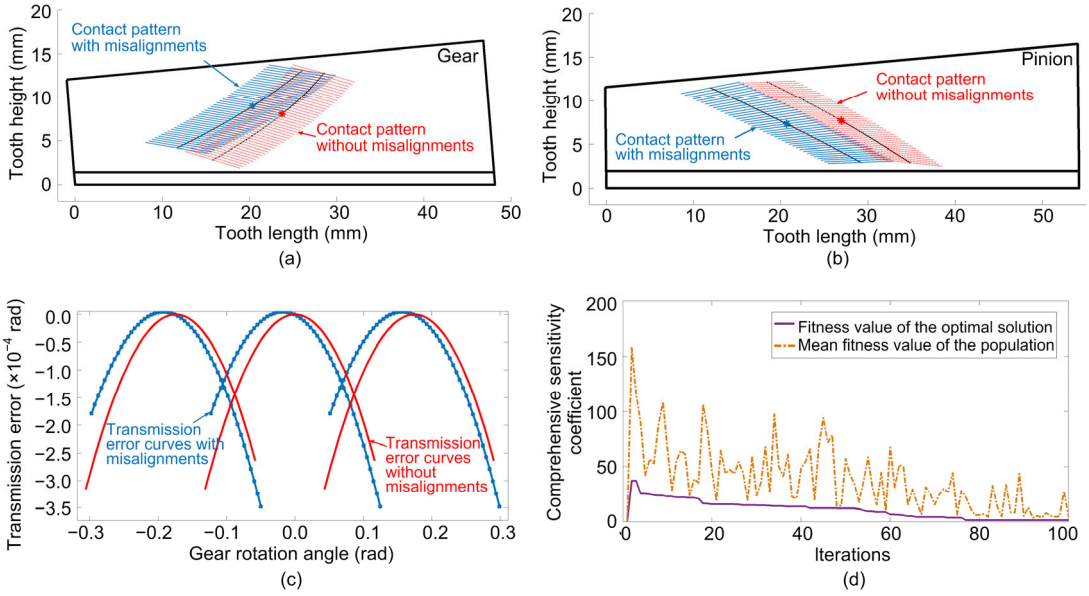

Fig. 16 Contact patterns on gear (a) and pinion (b), TE curves (c), and fitness curves (d) of the optimized gear pair

Table 11 Sensitivity coefficients of the optimized design

Misalignment	S_γ	S_s	S_x	S_y
H_G	−0.206 83 (−8.85%)	19.419 54 (−4.89%)	7.052 82 (−5.69%)	0.068 64 (3.40%)
H_P	−0.111 08 (−3.48%)	1.698 03 (−6.17%)	−13.776 01 (−1.79%)	−1.649 49 (−1.14%)
V	−0.414 91 (2.63%)	−5.636 28 (2.25%)	−31.638 41 (−9.35%)	−1.735 52 (0.65%)
Σ	−0.647 20 (−5.69%)	−44.743 01 (−8.17%)	−30.467 34 (−6.79%)	1.428 21 (4.83%)

equivalent misalignments has decreased. It must be noted that after optimization, the sensitivities of the direction angle, the area, and the vertical position to the offset error have increased respectively. The reason is that in the optimization process, the 16 sensitivity coefficients of the four indexes to the four kinds of misalignments are simultaneously optimized for decreasing. Through our research, we found that there are mutual constraints among these 16 coefficients, and the decline of some coefficients will lead to other factors rising. Thus, we can only find a Pareto optimal solution in the entire solution set. Table 11 gives the smallest coefficients set of the weighted sensitivities, so the most sensitive coefficients of horizontal position and area are reduced observably. Based on the obtained conclusion that the four indexes are most sensitive to the angular error, and secondly to the offset error, it can be concluded that this optimization achieves the goal of reducing the comprehensive sensitivity. According to the sensitivity analysis, the assembly accuracy of the angle between the crossed axes and the offset should be controlled first in future work to reduce these sensitivities. The effects of the stiffness and the wear of the bearings, the deformation of the shafts, and the eccentricity of the gear will also be considered in a detailed study in the future. Table 12 gives the original and optimized machine-tool settings.

Table 12 Machine-tool settings of the pinion in two cases

Item	Value	
	Original	Optimized
Tilt angle, i (°)	2.049 92	2.017 77
Swivel angle, j (°)	263.932 88	255.924 51
Basic cradle angle, q (°)	73.629 35	77.802 52
Radial setting, S_r (mm)	145.784 92	139.954 23
Blank offset, ΔE_m (mm)	49.45	46.561 60
Sliding base, ΔX_B (mm)	10.09	7.756 24
Machine center to back, ΔX_D (mm)	−6.34	−5.693 00
Machine root angle, γ_m (°)	10.35	10.28
Cutting ratio, m_{cp}	5.507 13	5.233 84

8 Conclusions

The effects of four kinds of misalignments on the contact patterns of a pair of mismatched hypoid gears have been investigated in this study. The models and optimization framework established in this paper can be summarized as: (1) an accurate parametrized measurement model of the contact pattern; (2) a comprehensive sensitivity model of the contact pattern to misalignments; (3) an optimization framework consisting of the calculated model of the machining parameters, a TCA considering alignment errors, and a misalignment sensitivity evaluation model. There are some meaningful observations in this study which are presented as follows:

1. The influence rules of the four different misalignments on the contact pattern are different. Taking the researched gear pair as the example, the evaluation indexes are most sensitive to the angular error between the pinion shaft and the gear shaft. Therefore, in the installation process of the hypoid gear pair, an angular error should be avoided as much as possible. The influence of the running offset error is also significant, while the impact of the axial misalignment of the gear is minimal, followed by the axial misalignment of the pinion.

2. By optimizing the sensitivity of the contact pattern to the four equivalent misalignments, the sum of the sensitivity coefficients of the evaluation indexes has been reduced, the sensitivity of meshing performance to misalignments has also been reduced, thereby improving the meshing stability of the gear pair. The improved MPGA algorithm can achieve the expected goal with a good convergence rate.

3. Sensitivity analysis and optimization of the contact pattern of hypoid gears to misalignments have prospect of wide application in meshing quality control, and the design of the tolerance zone and the optimal structure. By the AE-TCA approach, considering the alignment errors of a hypoid gear pair, the influence rule and the tolerance law of the installation errors on the contact quality can be obtained. The conclusion provides a basis for the process and installation of hypoid gears and a reference for the manufacture of bearings and powertrain reducers.

References

Achtmann J, Bär H, 2003. Optimized bearing ellipses of hypoid gears. *Journal of Mechanical Design*, 125(4):739-745. https://doi.org/10.1115/1.1625403

ANSI-AGMA, 2005. Design Manual for Bevel Gears, ANSI/AGMA 2005-D03. National Standards of America, USA.

ANSI-AGMA, 2008. Assembling Bevel Gears, ANSI/AGMA 2008-C01. National Standards of America, USA.

Artoni A, Bracci A, Gabiccini M, et al., 2008. Optimization of the loaded contact pattern in hypoid gears by automatic topography modification. *Journal of Mechanical Design*, 131(1):011008. https://doi.org/10.1115/1.3013844

Baxter ML, Spear GM, 1961. Effect of misalignment on tooth action of bevel and hypoid gears. ASME Design Conference, ASME 61-MD-20.

Bracci A, Gabiccini M, Artoni A, et al., 2009. Geometric contact pattern estimation for gear drives. *Computer Methods in Applied Mechanics and Engineering*, 198(17-20):1563-1571. https://doi.org/10.1016/j.cma.2009.01.009

Deng XZ, Wei BY, 2012. The New Methodology of the Bevel Gear's Design. Science Press, Beijing, China (in Chinese).

Ding H, Zhou YS, Tang JY, et al., 2016. A novel operation approach to determine initial contact point for tooth contact analysis with errors of spiral bevel and hypoid gears. *Mechanism and Machine Theory*, 109:155-170. https://doi.org/10.1016/j.mechmachtheory.2016.11.007

Elisaus V, Mohammadpour M, Theodossiades S, et al., 2017. Effect of teeth micro-geometrical form modification on contact kinematics and efficiency of high performance transmissions. *Proceedings of the Institution of Mechanical Engineers, Part K: Journal of Multi-body Dynamics*, 231(3):538-555. https://doi.org/10.1177/1464419317710157

Fan Q, 2011. Optimization of face cone element for spiral bevel and hypoid gears. *Journal of Mechanical Design*, 133(9):091002. https://doi.org/10.1115/1.4004546

Fan Q, Wilcox L, 2007. New developments in tooth contact analysis (TCA) and loaded TCA for spiral bevel and hypoid gear drives. *Gear Technology*, 24(3):26-35.

Gabiccini M, Bracci A, Guiggiani M, 2010. Robust optimization of the loaded contact pattern in hypoid gears with uncertain misalignments. *Journal of Mechanical Design*, 132(4):041010. https://doi.org/10.1115/1.4001485

Guo WC, Mao SM, Yang Y, et al., 2016. Optimization of cutter blade profile for face-hobbed spiral bevel gears. *The International Journal of Advanced Manufacturing Technology*, 85(1-4):209-216. https://doi.org/10.1007/s00170-015-7893-5

Hotait MA, Kahraman A, Nishino T, 2011. An investigation of root stresses of hypoid gears with misalignments. *Journal of Mechanical Design*, 133(7):071006. https://doi.org/10.1115/1.4004224

Kolivand M, Kahraman A, 2009. A load distribution model for hypoid gears using ease-off topography and shell theory. *Mechanism and Machine Theory*, 44(10):1848-1865. https://doi.org/10.1016/j.mechmachtheory.2009.03.009

Litvin FL, Fuentes A, 2004. Gear Geometry and Applied Theory (2nd Edition). Cambridge University Press, New York, USA.

Litvin FL, Tsung WJ, Lee HT, 1987. Generation of Spiral Bevel Gears with Conjugate Tooth Surfaces and Tooth Contact Analysis. NASA Contractor Report No. 4088, National Aeronautics and Space Administration, USA.

Litvin FL, Zhang Y, Handschuh RF, 1991. Local Synthesis and Tooth Contact Analysis of Face-milled Spiral Bevel Gears. NASA Contractor Report No. 4342, National Aeronautics and Space Administration, USA.

Litvin FL, Chen JS, Sep TM, et al., 1995. Computerized simulation of transmission errors and shift of bearing contact for face-milled hypoid gear drive. *Journal of Mechanical Design*, 117(2A):262-268. https://doi.org/10.1115/1.2826133

Mermoz E, Astoul J, Sartor M, et al., 2013. A new methodology to optimize spiral bevel gear topography. *CIRP Annals*, 62(1):119-122. https://doi.org/10.1016/j.cirp.2013.03.067

Mohammadpour M, Theodossiades S, Rahnejat H, et al., 2014. Transmission efficiency and noise, vibration and harshness refinement of differential hypoid gear pairs. *Proceedings of the Institution of Mechanical Engineers, Part K: Journal of Multi-body Dynamics*, 228(1):19-33. https://doi.org/10.1177/1464419313496559

Pourvaziri H, Naderi B, 2014. A hybrid multi-population genetic algorithm for the dynamic facility layout problem. *Applied Soft Computing*, 24:457-469. https://doi.org/10.1016/j.asoc.2014.06.051

Simon V, 1996. Tooth contact analysis of mismatched hypoid gears. *American Society of Mechanical Engineers, Design Engineering Division (Publication) DE*, 88:789-797.

Simon V, 1998. The influence of misalignments on mesh performances of hypoid gears. *Mechanism and Machine Theory*, 33(8):1277-1291. https://doi.org/10.1016/S0094-114X(98)00005-6

Simon V, 2008. Machine-tool settings to reduce the sensitivity of spiral bevel gears to tooth errors and misalignments. *Journal of Mechanical Design*, 130(8):082603. https://doi.org/10.1115/1.2936903

Simon VV, 2014. Optimal tooth modifications in face-hobbed spiral bevel gears to reduce the influence of misalignments on elastohydrodynamic lubrication. *Journal of Mechanical Design*, 136(7):071007. https://doi.org/10.1115/1.4026264

Stadtfeld HJ, 1993. Handbook of Bevel and Hypoid Gears. Gleason Works, Rochester Institute of Technology, New York, USA.

The Gleason Works, 1971. Method for Designing Hypoid Gear Blanks. The Gleason Works, Rochester, USA.

Vivet M, Mundo D, Tamarozzi T, et al., 2018. An analytical model for accurate and numerically efficient tooth contact analysis under load, applied to face-milled spiral bevel gears. *Mechanism and Machine Theory*, 130:137-156. https://doi.org/10.1016/j.mechmachtheory.2018.08.016

Vogel O, Griewank A, Bär G, 2002. Direct gear tooth contact

analysis for hypoid bevel gears. *Computer Methods in Applied Mechanics and Engineering*, 191(36):3965-3982. https://doi.org/10.1016/s0045-7825(02)00351-1

Wang P, Zhang YD, Wan M, 2016. Global synthesis for face milled spiral bevel gears with zero transmission errors. *Journal of Mechanical Design*, 138(3):033302. https://doi.org/10.1115/1.4032471

Wang Q, Zhou C, Gui LJ, et al., 2018. Optimization of the loaded contact pattern of spiral bevel and hypoid gears based on a Kriging model. *Mechanism and Machine Theory*, 122:432-449. https://doi.org/10.1016/j.mechmachtheory.2018.01.008

Wang XC, Ghosh SK, 1994. Advanced Theories of Hypoid Gears. Elsevier, Amsterdam, The Netherlands.

Wu XT, 2009. Gear Engagement Principle (2nd Edition). Xi'an Jiaotong University Press, Xi'an, China (in Chinese).

Xu H, Kahraman A, 2007. Prediction of friction-related power losses of hypoid gear pairs. *Proceedings of the Institution of Mechanical Engineers, Part K: Journal of Multi-body Dynamics*, 221(3):387-400. https://doi.org/10.1243/14644193jmbd48

Zeng T, 1989. Design and Manufacture of Spiral Bevel Gear. Harbin Institute of Technology Press, Harbin, China (in Chinese).

Zhuo YB, Xiang XY, Zhou XJ, et al., 2017. A method for the global optimization of the tooth contact pattern and transmission error of spiral bevel and hypoid gears. *Journal of Zhejiang University-SCIENCE A (Applied Physics & Engineering)*, 18(5):377-392. https://doi.org/10.1631/jzus.A1600240

中文概要

题　目： 准双曲面齿轮接触印痕对安装误差的敏感性分析与优化设计

目　的： 准双曲面齿轮副在实际装配过程中不可避免地存在安装误差。本文旨在建立考虑多种安装误差的准双曲面齿轮啮合模型，对齿轮副啮合印痕特征（齿面分布位置、大小和方向）进行参数化建模，精确评价印痕对安装误差的敏感性，以及研究降低接触性能对安装误差的敏感度的方法，为准双曲面齿轮副的加工和安装提供理论依据。

创新点： 1. 对准双曲面齿轮齿面接触印痕进行精确的参数化建模；2. 建立考虑轴交角误差、偏置距误差以及大小轮轴向误差的齿轮副啮合分析模型；3. 建立准双曲面齿轮副安装误差敏感度综合评价模型；4. 通过优化齿轮加工参数，在齿轮副设计环节实现齿轮副安装误差敏感度的降低。

方　法： 1. 对准双曲面齿轮副安装误差和齿面接触印痕进行参数化建模，推导出表示接触印痕大小、方向和齿面分布位置的解析表达式（公式（1）~（3））；2. 建立考虑 4 种安装误差的准双曲面齿轮副啮合分析模型（公式（4）~（11）），得到不同安装误差对啮合印痕的影响（图 5~7）；3. 建立准双曲面齿轮副安装误差综合敏感度优化模型（公式（15）），并基于改进的多种群遗传算法（图 14）实现齿轮副安装误差敏感性的降低（图 8）。

结　论： 1. 四种安装误差对准双曲面齿轮啮合质量的影响程度不同；其中轴交角误差的影响最大，其次是偏置距误差，而大小轮的轴向安装误差的影响最小，因此安装齿轮副必须注重轴交角及偏置距的安装精度。2. 通过降低齿轮副安装误差综合敏感度，可在一定程度上降低系统对装配误差的敏感性；在齿轮副设计环节加入安装误差敏感度分析，优化机床加工参数，对装配后的啮合质量控制具有积极意义。3. 考虑安装误差的轮齿接触分析模型能够得到不同安装误差对啮合印痕及传动误差的影响规律，是一种对失配状态下的准双曲面齿轮副进行无载啮合分析的有效工具。

关键词： 准双曲面齿轮；失配；轮齿接触分析；敏感性分析；多种群遗传算法；多目标优化